Sheffield Hallam University

Influence of different types of solvent on the effectiveness of nanolime treatments on highly porous mortar substrates

OTERO, Jorge, STARINIERI, Vincenzo <http://orcid.org/0000-0002-7556-0702>, CHAROLA, A.E. and TAGLIERI, Giuliana

Citation:

Influence of different types of solvent on the effectiveness of nanolime treatments on highly porous mortar substrates

J. Otero[a*], V. Starinieri[a], A. E. Charola[b], G. Taglieri[c]

[a] Materials and Engineering Research Institute, Sheffield Hallam University, Sheffield, S1 1WB, UK

[b] Museum Conservation Institute, Smithsonian Institution, Washington DC, USA

[c] Department of Industrial and Information Engineering and Economics, University of L'Aquila, 67100 L'Aquila, Italy.

* corresponding author: Tel: +44 1142253500; Fax: +44 114 225 3501; jorge.otero.h@gmail.com.

Abstract. Historic calcareous structures suffer from weathering processes that result in the loss of some of their original properties. Nanolime products represent an attractive choice for the consolidation of these substrates containing calcite due to their high chemical compatibility with the original structure. The effectiveness of nanolime products has been widely proven for superficial consolidation treatments (e.g. plasters and wall-paintings). However, its consolidation mechanism in highly porous substrates (e.g. limestones or lime mortars) still needs to be fully understood. The aim of this paper is to study the influence of different types of solvent on the effectiveness of nanolime treatments on highly porous lime-mortars. The consolidation effectiveness is investigated by evaluating changes on superficial cohesion, porosity, drilling resistance, water absorption by capillarity, drying rate and aesthetic properties. Results showed that nanolime dispersed in a mixture of isopropanol (50%) and water (50%) yielded slightly better consolidation properties in terms of reduction in porosity, increase in strength and penetration within coarse lime-mortars than nanolime dispersed in other solvents.

1. Introduction

Over time, building materials can undergo decay processes as a result of the action of atmospheric agents which can lead structures to lose their mechanical properties [1]. Consolidant products are used to recover the mechanical properties of the weathered substrate and should be compatible with the substrate [2].

29

The consolidation of historic calcareous materials still represents nowadays a challenge in the conservation field due to the lack of compatible, effective and durable consolidants for these materials. Silica-based consolidants such as Tetraethyl orthosilicate (TEOS) or Trimethoxymethylsilane (MTMOS) have been widely used in restoration treatments in the past due to their ease of application, initial strength and proven effectiveness in other substrates. However, in the case of calcareous substrates, the lack of chemical compatibility between them and the substrate lead to unsatisfactory long-term effectiveness, which in many cases can lead to unsatisfactory results on limestones and on marble due to the difficulty of bonding a silicate material to calcite [3-6]. An inorganic consolidant, consisting of a colloidal suspension of $Ca(OH)_2$ in water (limewater), was traditionally used due to the total chemical compatibility with the calcitic substrate. However, this treatment presents some important limitations, such as the introduction of large quantities of water (due to the low solubility of $Ca(OH)_2$ in water), the reduced impregnation depth and the very slow rate of the carbonation process, which in many cases lead to unsatisfactory treatments [7, 8]. In recent years, hydroxyapatite, calcium alkoxides or innovative materials based on nanocomposites of ethyl-silicate have also been tested with promising outcomes [9, 10], but further research needs to be undertaken to assess their long-term effectiveness.

44

Nanoparticles of $Ca(OH)_2$ (nanolimes) were developed and successfully tested for wall-paintings in 2001, overcoming the limitations of the traditional limewater treatment [11]. Nanolimes preserve the same compatibility of the traditional lime-water treatment while presenting superior consolidation properties to limewater due to the increase of lime particles introduced and to the reduced size of the particles. Nanolimes are colloidal alcoholic or hydro-alcoholic dispersions with higher reactivity and particle concentration, which can improve the consolidating action of the traditional limewater technique in terms of higher penetration, strength and reduction of the application time [12, 13]. Nanolimes have emerged as an efficient consolidant for the superficial consolidation of different historic substrates (e.g. wall-paintings, stuccos or plasters) [14] and for the conservation of other cultural heritage materials such as paper [15], canvas [16], bones [17] and wood [18]. However, the results obtained when applied to highly porous substrates are few and controversial [6, 19, 20] and its consolidation mechanism still needs to be fully understood particularly in relation with the penetration of nanoparticles into the highly porous network.

56

57 The effectiveness of nanolime in highly porous substrates can be influenced by several factors: i) low concentration

58 nanolime dispersion (e.g. 5 g/L) can reduce the accumulation of the particles at the surface thus helping the

59 penetration of nanoparticles into the pores [12, 21]; ii) repeated applications increase the consolidation

60 effectiveness [12, 22]; iii) high relative humidity environments (>75%RH) enhance the carbonation process [23]; iv)

61 the type of alcoholic solvent influences the rate of carbonation reaction and the formation of different polymorphs

62 of calcium hydroxide [23, 24]; v) the presence of residual water content in the nanolime suspension and a reduced

63 concentration of the nanolime dispersion enhance the carbonation process [24-26]; vi) nanolime particle size can

64 influence the consolidation effectiveness in relation with the substrate pore structure where larger particle size

65 nanolime tends to be deposited mainly in the large sized pores, while smaller particle size nanolime tends to fill

66 both large and small pores equally [27]; vii) nanolime storage conditions after synthesis (T< 5°C, for short periods

67 of time) reduce the conversion of $Ca(OH)_2$ into Ca-alkoxides which enhances the carbonation process [28].

68

69 Nanolimes are applied in a wide range of solvents (i.e. ethanol, propanol, butanol, water or a mixture of these

70 solvents) [12, 29-33]. In recent years, a series of studies suggested that the type of solvent could be critical for the

71 nanolime effectiveness in highly porous substrates [29, 30, 34]. These researches suggested that the deposition of

72 $Ca(OH)_2$ nanoparticles in the pores occurs during the solvent evaporation phase where most of the nanoparticles

73 could migrate back to surface [34]. The same authors also suggested that solvents with low evaporation rate (e.g.

74 water) could be more suitable for coarse porous substrates as they seem to reduce the back-migration of the

75 nanoparticles to the surface contributing to their deposition in-depth [29, 30].

76

77 The aim of this paper is to study the influence of different types of solvent on the effectiveness of nanolime

78 treatments on highly porous lime-mortars. In this experimental work, the $Ca(OH)_2$ nanoparticles were dispersed in

79 five solvents at the same concentration (5 g/L) following the same synthesis route and conditions. The

80 consolidation effectiveness of the resulting nanolime treatments was investigated by assessing changes in porosity,

81 superficial cohesion, drilling resistance, water absorption by capillarity, drying rate and aesthetic properties.

82

83 **2. Materials and methods**

84 *2.1 Lime mortar samples*

Mortar samples were manufactured from lime powder (Singleton Birch Ultralime CL90) and a fine silica sand (Pentney, UK) in a proportion of 1:2.5 (bulk volume) measured (constant flow of 16 cm) according to the European Standard BS EN 1015-3:1999 [35]. The water:binder ratio to obtain the desired flow was 1.56. Mortars were batched by weight after measuring lime and sand densities according to EN 1015-2:1998 [36]. Mortars were produced by mixing the dry ingredients with water in a Hobart mixer. The mix protocol was as follows: 1) dry mix sand and lime for 2 min at 62 rpm; 2) add water while continuing mixing at 62 rpm for 30 s; 3) stop the mixer for 30 s and scrape the mixer bowl; 4) mix for 5 min at 125 rpm. Samples were cast in 40 x 40 x 160 mm steel moulds in two layers and vibration-compacted. Immediately upon floating off the fresh mortar, the moulds were transferred to a temperature and humidity controlled room maintained at 20 ˚C and 65% RH. Mortar beams were cured at 5-15˚C and 60-80%RH for 28 days under monitored outdoor conditions. Upon completion of the curing period, each prism was cut into 4 cubes measuring approximately 40x40x40 mm which were cured for further 28 days in the same conditions.

The mortar's chemical composition was obtained by X-Ray Fluorescence (*Philips PW2400*). XRF samples consisted of pressed powder pellets (Retsch PP-40 pellet press) and the elemental weight percentages calculated from total oxide X-Ray analysis. XRF results shows that the lime mortar is composed by Si ($63.8\pm0.5\%$), Ca ($32.7\pm0.1\%$) and traces of Al ($1.2\pm0.3\%$), K ($1.0\pm0.3\%$) and P ($0.8\pm0.3\%$).

The mortar's mineralogical composition was obtained by X-Ray Diffraction (PANalytical XPert PRO) recorded with a step size of $0.026°2\theta$ in the angular range $20-70°2\theta$. X-ray data were fitted using the pseudo-Voigt profile function and refined by means of Rietveld refinement [37, 38]. XRD samples were ground and sieved (80 μm sieve mesh) and placed over an XRD zero-background sample holder prior to the XRD analysis. The XRD-Rietveld refinements show the mortar is composed of 79.9% Quartz (SiO_2, ICSD #00-046-1045) and 20.1% calcite ($CaCO_3$, ICSD #00-005-0586). XRD was not able to identify the presence of any other mineral phases (e.g. feldspar containing Al, K and P, which were elements detected by XRF) suggesting that any other mineral phases containing those elements could be present in amorphous or poorly crystallised phases or in amounts below the instrument detection level (< 1%).

113 The mortar's pore structure was determined by Mercury Intrusion Porosimetry (MIP) using a *PASCAL 140/240*

114 instrument. The samples for MIP consisted of two mortar fragments measuring approximately 8 x 8 x 15 mm taken

115 from the surface (up to a depth of 20 mm) of the sample, which were dried in an oven at 60 ℃ until constant weight.

116 The average porosity of the mortar measured by MIP was 23 ± 1.6 vol.% with a bulk density of 1.698 ± 0.1 g/cm^3.

117

118 *2.2 Synthesis and characterisation of nanolime*

119 Nanolime was synthesized through a patented process based on an ion exchange process between an anion

120 exchange resin (Dowex Monosphere 550A OH by Dow Chemical) and an aqueous calcium chloride solution

121 ($CaCl_2$ by Sigma-Aldrich), as described in the literature [39, 40, 41]. Following the synthesis, the newly

122 synthetized nanoparticles of $Ca(OH)_2$ were dispersed in five solvents at the same concentration (5 g/L):

123 Isopropanol (IP), Ethanol (ET), Water (W), 50-50% Water-Isopropanol (WIP) and 50-50% Water-Ethanol (WET).

124 A small residual water (W = 5%) was left intentionally in the suspension of IP and ET, as this practice enhances the

125 carbonation process [26, 42]. The relevant properties of the solvents are reported in Table 1. Suspensions were kept

126 in a refrigerator (T < 5 °C) prior the application to minimize the $Ca(OH)_2$ particles conversion into Ca alkoxides

127 [28, 43].

128

Table 1. Physical-chemical properties of the selected nanolimes

Code	Solvent	g/L	Boiling point (℃)	Surface tension (solvent/air) (N/m)	Treated Samples
IP	Isopropanol	5	82.6	0.0230	3
ET	Ethanol	5	78.3	0.0221	3
W	Water	5	99.6	0.0728	3
WIP	50-50% Water-Isopropanol	5	87.3	0.0247	3
WET	50-50% Water-Ethanol	5	92.2	0.0281	3

129

130 The size and shape of the synthetized nanolime particles was determined by TEM (Philips CM200) while their

131 crystalline phases were analysed by XRD (PANalytical X'PertPRO). Both TEM and XRD were carried out

132 immediately after the synthesis and samples were prepared in nitrogen atmosphere (99.99% nitrogen gas) TEM

133 samples were prepared by placing a few drops of the primary nanolime suspension (W) on a TEM carbon-coated

134   copper grid while XRD samples were prepared by dispersing 0.12 ml of each suspension in an XRD silica sample

135   holder.

136

137   The relative kinetic stability (KS) of the suspensions was determined from the variation over time (2 hours) of their

138   absorbance (at $\lambda = 600$ nm) using a UV/VIS Spectrophotometer (UV-VIS Spectrophotometer Varian 50SCAN).

139   Nanolimes were agitated before the test to increase their colloidal stability [12]. The KS % was calculated using the

140   following formula:

141   $$KS \% = 1 - [(A_0 - A_t)/A_0] \times 100$$

142   where A_0 is the starting absorbance and A_t the absorbance at time t, both at a wavelength of 600 nm as described in

143   literature [12, 43].

144

145   The surface tension of the solutions was determined by the pendant drop method using an OCA 15 Plus instrument

146   (Dataphysics). For this test, a solution drop (5 µL) was pendant through a Hamilton 50 µL DS 500/GT syringe. The

147   surface tension of the nanolime was calculated by measuring the shape of the pendant drop of the dosing needle,

148   defined with the Young–Laplace equation:

$$AP = \gamma \left(\frac{1}{R1} + \frac{1}{R2} \right)$$

149

150   where ''ΔP'' is the difference in pressure across the interface, ''γ'' the surface tension, and ''R1'' and ''R2''are

151   the curvature radius [44].

152

153   *2.3 Nanolime carbonation study*

154   The influence of the solvent in the carbonation process was investigated by XRD. Samples were prepared by

155   exposing 0.12 ml of each suspension to outdoor conditions (T ≈ 5-15˚C, R.H ≈ 60-80%) for 1 hour and for 7 days.

156   XRD data was recorded with a step size of $0.026°2\theta$ in the angular range 15-70°2θ and data were fitted and refined

157   as described in section 2.1.

158

159   *2.4 Nanolime treatments*

160 The treatments were carried out by brush in outdoor conditions (T ≈ 5-15˚C, R.H ≈ 60-80%) in a protocol applied

161 in previous studies [12, 27, 44]. Treatment started two days after the synthesis to reduce the conversion of $Ca(OH)_2$

162 into Ca-alkoxides and improve their effectiveness [28]. Each nanolime (IP, ET, W, WIP and WET) was agitated

163 before each brushstroke and applied on the top face (as cast) surface of three mortar cubes (40 x 40 x 40 mm) per

164 each nanolime. The application was stopped when no absorption was observed (samples reached constant weight

165 and the surface remained completely wet without absorption for a period of at least 1 minute). After saturation, the

166 samples were left to dry and retreated again after 48 hours, when samples were completely dry. Samples were

167 weighed before and after each application (dry weight and saturated weight) to measure the amount of nanolime

168 absorbed by each mortar cube during each application. The treatment was terminated when each cube absorbed 500

169 mg of calcium hydroxide (approximately 100ml) which required approximately 40 days (20 days of nanolime

170 application). Following the treatment, the samples were cured at RH ≈ 60-80%RH under controlled outdoor

171 conditions for 28 days prior to the analysis. A set of Control samples (CO) were kept in the same controlled

172 outdoor conditions for the same period.

173

174 *2.5 Treatment drying rate*

175 The drying rate of the treatments was evaluated by measuring the weight loss over time after saturation of three

176 treated samples per each suspension, in accordance with the EN Standard [45]. The aim of this test is to determine

177 the evaporation rate of each nanolime suspension in order to investigate possible correlations of the solvent

178 evaporation rate with the consolidation effectiveness, as suggested by previous authors [30]. This test was carried

179 out under controlled outdoor conditions (T ≈ 5-15˚C, R.H ≈ 60-80%).

180

181 *2.6 Consolidation effectiveness*

182 Following curing, the consolidation effectiveness was analysed by means of the following techniques and methods.

183 MIP was carried out to measure the influence of the treatments on open porosity and pore size distribution.

184 Samples for MIP were taken from the mortar's surface (up to a depth of 50 mm) of both treated and control

185 samples.

186

187 Water absorption coefficient (WAC) was measured according to EN 13755 [46]. Upon completion of this test, the

188 samples were totally immersed in water for 24 hours at room atmosphere and the drying behaviour of the samples

189 was also measured [47]. Three cubes per treatment were tested for both treated and control samples.

190

191 'Scotch Tape Test' (STT), according to ASTM 2009 [48], was carried out to measure the influence of the

192 treatments on surface cohesion. Nine measures per treatment were obtained for both treated and control samples.

193

194 Drilling Resistance Measurement System (DRMS) (SINT-Technology) was carried out to obtain the depth of

195 penetration of each nanolime and their influence on strength. The DRMS was specifically designed for assessing

196 the penetration and effectiveness of consolidants in homogeneous substrates [20]. DRMS tests were carried out

197 using a new drill bit of 5 mm diameter per each sample, rotation speed of 200 rpm, penetration rate 15 mm/min and

198 penetration depth of 20 mm. Six measurements were performed for both control and treated samples and their

199 mean curve was calculated for comparison.

200

201 Scanning Electron Microscope (SEM, NanoSEM 450) was used to observe the surface of both treated and control

202 samples. Samples for SEM were coated with a 20nm thick layer of gold using a Quorum Q150T. SEM images were

203 obtained with an ETD detector, a working distance of 3mm, an accelerating voltage of 15 kV and a spot size of 30

204 nm.

205

206 Colorimetric analysis (Minolta CM508D Colorimeter) was undertaken to determine any possible surface colour

207 changes induced by the nanolime treatments. Previous researches reported a whitening appearance after nanolime

208 treatments [12, 32] and this research aims to observe differences regarding the type of solvent used. Thirty

209 measurements were obtained for each control and treated samples, which were taken on random areas of the sample

210 surfaces. Total colour variation (ΔE) was calculated by the formula:

$$\Delta E^* = \sqrt{\Delta L^{*2} + \Delta a^{*2} + \Delta b^{*2}}$$

211 where ΔL* is the change in lightness (white-black parameter), Δa* (red-green parameters) and Δb* (blue-yellow

212 parameters).

213

3. Results and Discussions

3.1 Characterization of the nanolime suspensions

The TEM photomicrograph in Fig. 1 shows a plate-like hexagonal $Ca(OH)_2$ nanoparticle. This morphology is identical to that observed for nanolime particles analysed in previous studies, which we also synthetized by anion exchange processes [12, 32]. These $Ca(OH)_2$ nanoparticles are regularly shaped and have diameters ranging from 20 to 80 nm, which is also in line with previous research on the same type of nanolime [16, 31, 32].
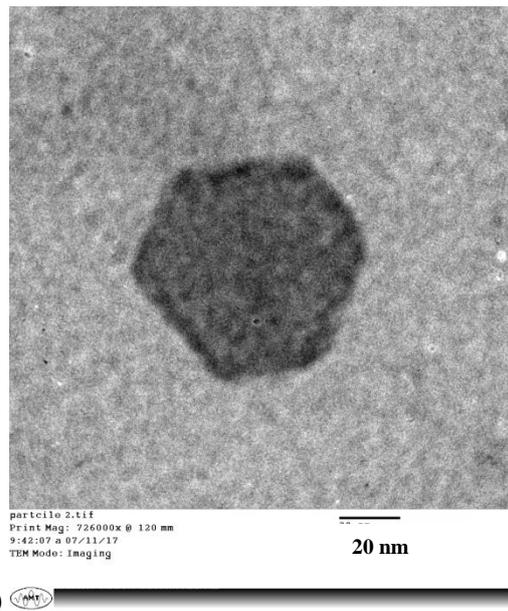
Figure 1. TEM micrograph of a small single particle of synthesised nanolime (IP)

XRD analysis of samples dried in nitrogen atmosphere (Fig.2) show that the only crystal phase present in all suspensions corresponds to Portlandite ($Ca(OH)_2$, ICSD #01-087-0674) except for the W sample (nanolime in water) which contains an approximately 20% amount of calcite (ICSD #01-072-1652). This is attributed to the higher reactivity of the $Ca(OH)_2$ nanoparticles with CO_2 when dispersed in water, as moisture significantly contributes to the carbonation process [26, 31, 33]. Rietveld refinement showed that the W sample consists of 79.3% Portlandite and 20.7% Calcite. For all samples, the strongest peak corresponds to the {001} basal plane. IP, ET, WIP and WEP dry particles have a preferred orientation to the planes {010} or {100}, which are both side planes. The Rietveld refinement factors are included in Table 2.

Table 2. Rietveld refinement factors of samples dried in Nitrogen atmosphere

| | Nitrogen | | | | |
	IP	ET	W	WIP	WET
R-expected	10.1	9.3	13.1	18.4	13.8
R-profile	11.6	7.9	14.5	15.4	11.7
Weighed R profile	14.6	10.3	12.7	11.1	16.1
Goodness of fit	3.4	3.3	4	4.1	4.3
Phase proportions	100% P	100% P	79.3%P 20.7%C	100% P	100% P
Direction of preferred orientations	010	100	NPO	010	100

NPO (No preferred orientation), P (Portlandite); C Calcite)

233

234

235 a)

236 c)

d)

237 e)
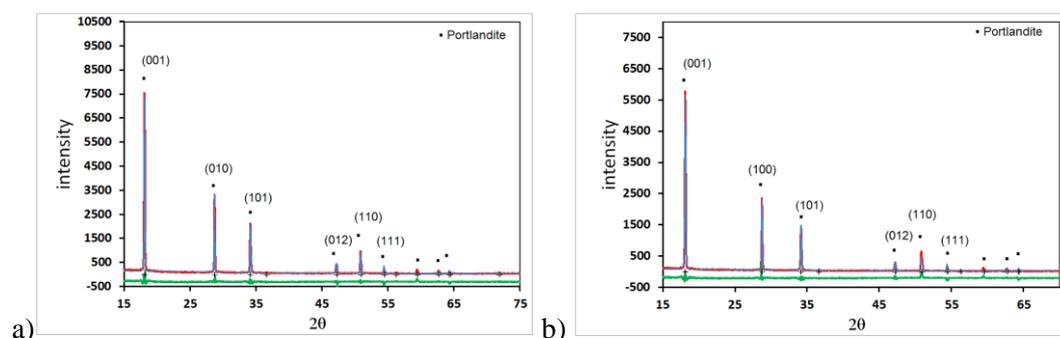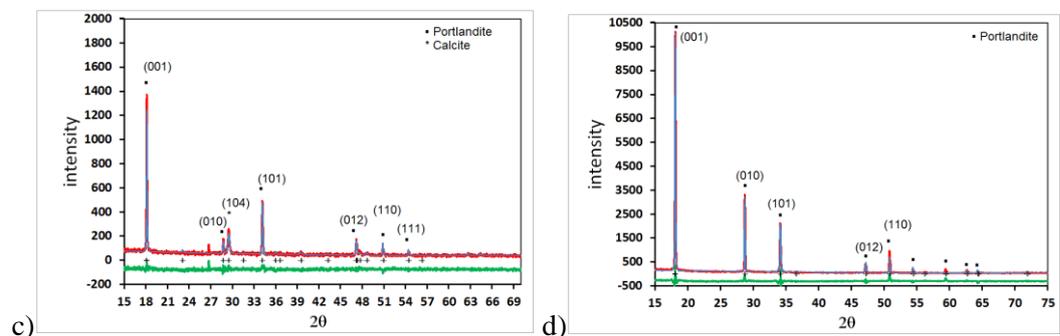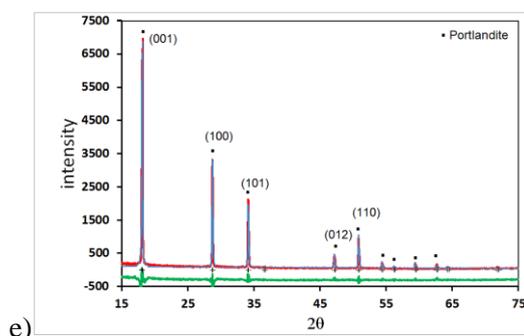
Figure 2. XRD patterns of samples dried under nitrogen atmosphere for; a) IP (Isopropanol); b) E (ethanol); c) W (water); d) WIP (50% Water and 50% Isopropanol); and e) WET (50% water and 50% Ethanol). Red line corresponds to Intensity observed, blue line to Intensity calculated and green line to the Intensity observed - Intensity calculated difference curve. The crystal phases are shown in brackets and the "+" symbol corresponds to the main peaks. In parentheses, the Bragg peaks indexes of portlandite.

243

244
245 Figure 3 shows the colloidal stability of IP, ET, W, WIP and WET suspensions over a period of 2 hours following a

246 moderate agitation. WIP presented the highest colloidal stability (settling speed ≈ 5% per h). Similar results were

247 observed in previous studies carried out on this type of nanolime suspension [12, 31, 32]. The colloidal stability of

248 alcoholic nanolime dispersions synthesised by anionic exchange process is lower than that of nanoparticles

249 synthesised by other routes (e.g. solvothermal reactions or drop-to-drop method), where nanoparticles remain in

250 colloidal state for more than one week [11, 18, 29]. Nevertheless, all dispersions showed a reasonable colloidal

251 stability where most of the nanoparticles (>95%) remain in colloidal state during the first 5-10 minutes after

252 agitation, which is considered acceptable in terms of practical purposes [12].

253
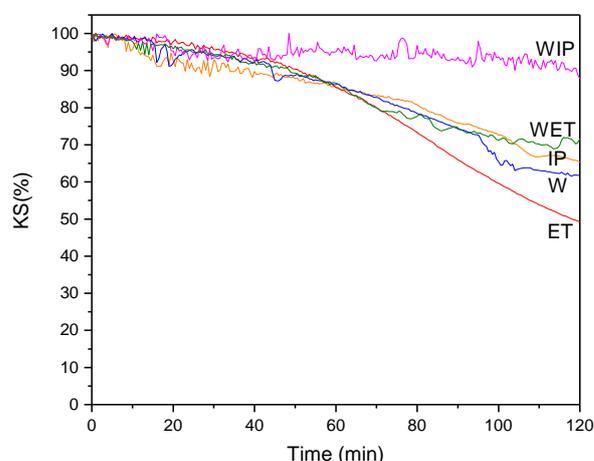
254 **Figure 3.** Kinetic stability KS (%) of IP (Isopropanol), E (ethanol), W (water), WIP (50% Water and 50% Isopropanol) and
255 WET (50% water and 50% Ethanol) samples
256

257

258 *3.2 Nanolime carbonation study*

259 The XRD analysis of the nanolime suspensions exposed to air for 1 hour (60-80% RH) proved the high reactivity

260 of the nanoparticles (Fig. 4), independently from the solvent. Calcite (ICSD # 01-085-1108) is the only crystalline

261 phase detected for all suspensions. W sample (Water) showed a better developed crystalline structure (Fig. 4c)

262 which confirms the higher reactivity of the $Ca(OH)_2$ nanoparticles when suspended in water. The Rietveld

263 refinement factors are included in Table 3.

Table 3. Rietveld refinement factors of samples exposed to air in outdoor conditions (60-80%RH) for 1h and 7 days.

	1 hour in air		7 days in air

	IP	ET	W	WIP	WET	IP	ET	W	WIP	WET
R-expected	15.8	15.2	14.7	14.7	14.9	15.7	15.3	21.2	15.6	14.8
R-profile	11.3	10.7	12.3	11.4	9.9	11.1	11.3	16.1	16.3	10.8
Weighed R profile	14.3	13.6	16.2	14.5	12.7	14.1	14.1	20.8	20.8	13.7
Goodness of fit	1.8	1.8	1.2	1.9	1.7	1.8	1.8	1.9	1.7	1.8
Phase proportions	100% C	100% C	100% C	100% C	100% C	100% C	100% C	100% C	100% C	100% C
Direction of preferred orientations	NPO	NPO	NPO	NPO	NPO	104	104	104	104	104

NPO (No preferred orientation), P (Portlandite); C (Calcite)

264


265 a)

266 c) d)

267 e)
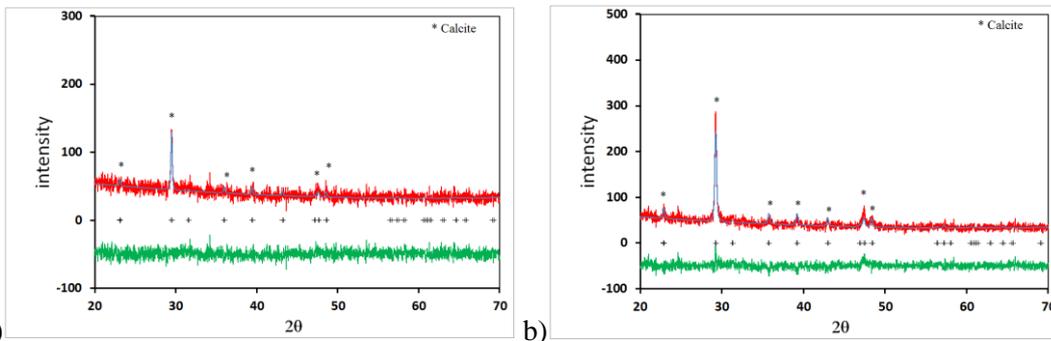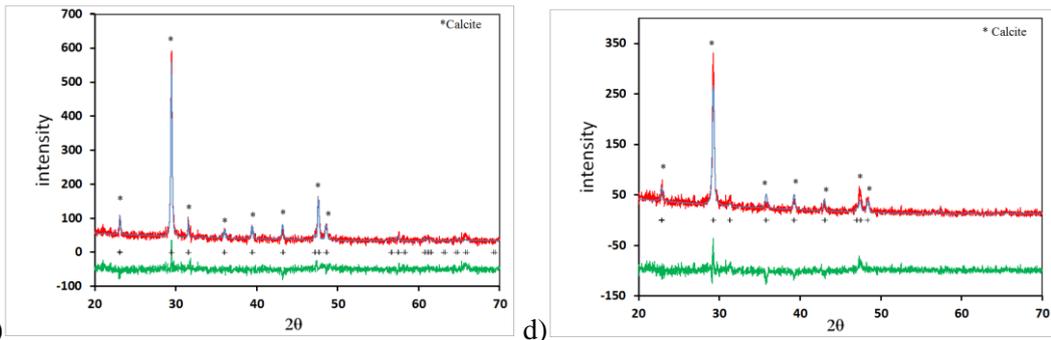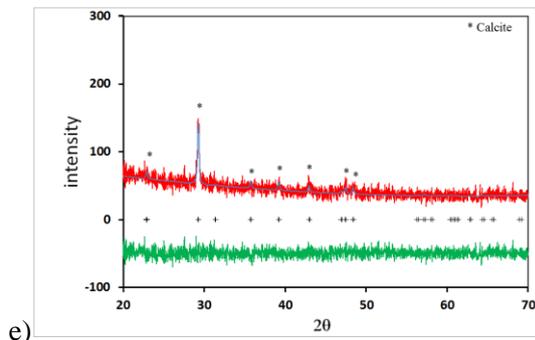
268 **Figure 4**. XRD patterns after 1 hour of air exposure (60-80%RH) for; a) IP (Isopropanol); b) E (ethanol); c) W (water); d) WIP
269 (50% Water and 50% Isopropanol); and e) WET (50% water and 50% Ethanol). Red line corresponds to Intensity observed,
270 blue line to Intensity calculated and green line to the Intensity observed - Intensity calculated difference curve. The crystal
271 phases are shown in brackets and the "+" symbol corresponds to the main peaks.
272

273

274 The XRD results after 7 days of air exposure (Fig. 5) show that all samples are composed of pure calcite crystals

275 (CaCO$_3$, ICSD# 01-086-2334) oriented to {104}, similar to that reported in previous studies [12, 31]. The low

276 intensity recorded for the IP (Isopropanol) sample (Fig. 5a) suggests this sample presents a slightly poorer

277 crystalline phase. The Rietveld refinement factors are included in Table 3.

278

279 a)   b)

280 c)   d)

281 e)
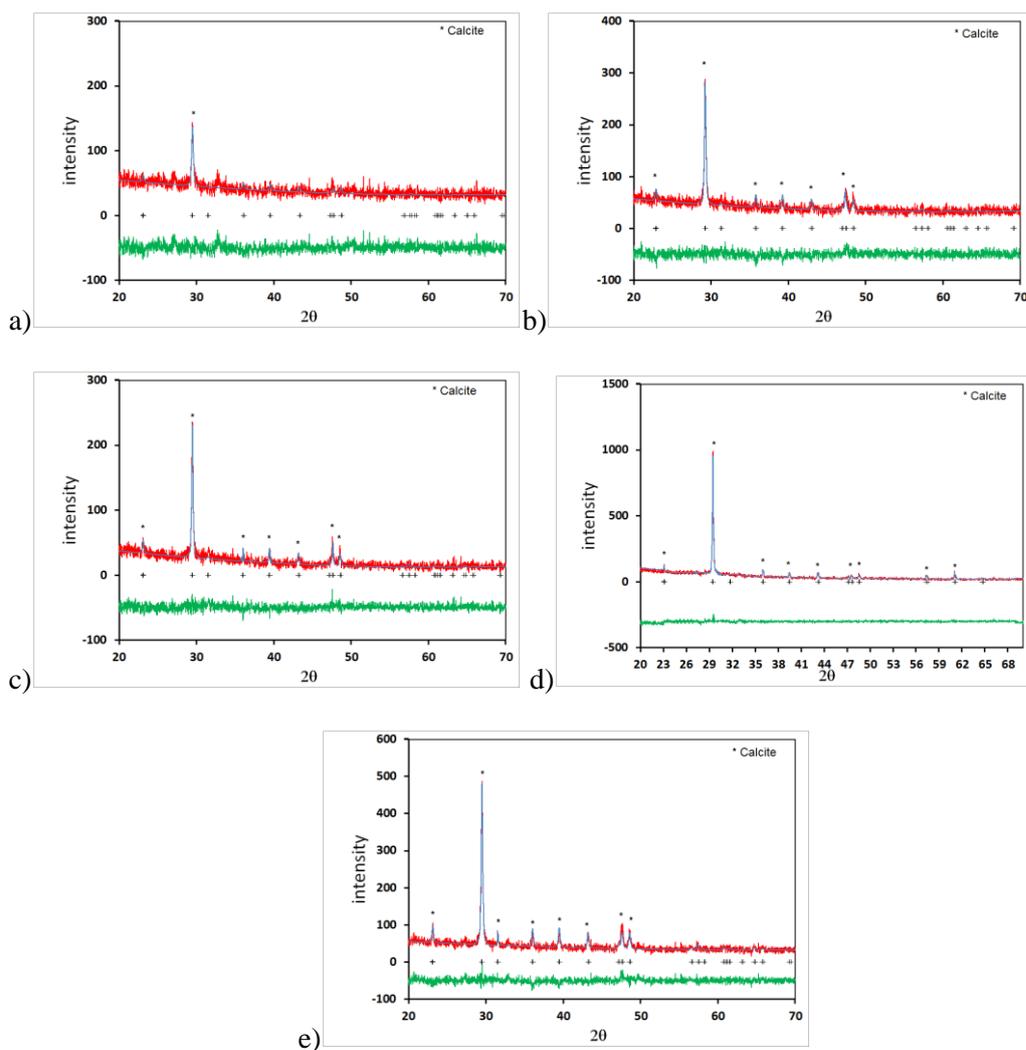
282 **Figure 5**. XRD patterns after 7 days of air exposure (60-80%RH) for; a) IP (Isopropanol); b) E (ethanol); c) W (water); d) WIP
283 (50% water and 50% Isopropanol); and e) WET (50% water and 50% Ethanol). Red line corresponds to Intensity observed,
284 blue line to Intensity calculated and green line to the Intensity observed - Intensity calculated difference curve. The crystal
285 phases are shown in brackets and the "+" symbol corresponds to the main peaks.
286

287

288 *3.3 Treatment drying rate*

289 Figure 6 shows the evaporation kinetics of the nanolimes after their application. ET and IP treatments evaporated

290 faster compared to the other treatments, which can be attributed to the lower boiling point of ethanol and

291   isopropanol (Table 1). Both solvents completely evaporated in approximately 24 hours. In contrast, WIP and WET

292   treatments required approximately 28 hours. This could be attributed to the fact that both isopropanol and ethanol

293   form azeotropic mixtures with water (87,7% and 95.4% alcohol respectively) with the latter having a lower boiling

294   point (78.4ºC) than the isopropanol one (82.6ºC). The W sample took some 48 hours to dry. The evaporation of W

295   treatment is slower due to the higher surface tension of water that enhances its retention within the pore network,

296   delaying the drying rate [30, 49].

297

298
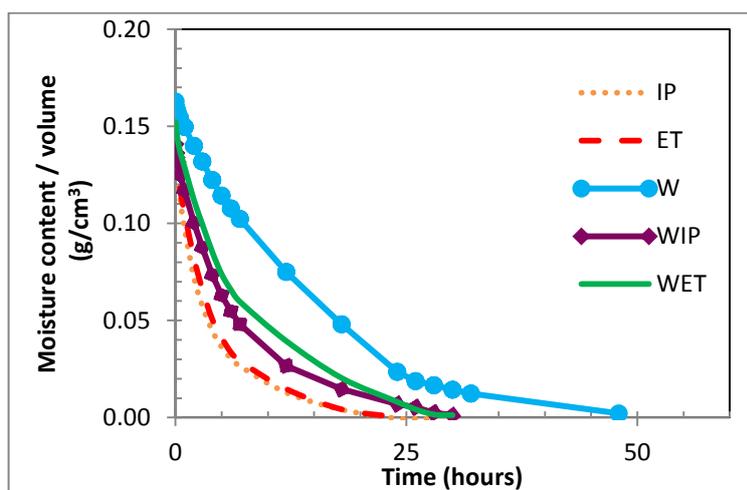
299   **Figure 6.** Drying kinetic curves for the treated mortars
300

301

302   *3.4 Consolidation effectiveness*

303   The porosity and pore structure properties of the control and treated mortars are summarised in Table 4. All

304   treatments caused a slight reduction in the porosity of the mortar near the surface (samples taken within 50 mm

305   from the surface), apart from IP sample where the standard deviation makes this difference statistically

306   insignificant. WIP yielded a slightly higher reduction in porosity (23% reduction), followed by W (17%), compared

307   to the other treatments (from 6 to 12%). All samples showed an increased total pore surface area (m^2/g), suggesting

308   the presence of a higher amount of smaller pores after treatment, as confirmed from the MIP curves (Fig. 7).

Table 4. Porosity properties of treated and untreated samples. CO*: control sample, numbers in brackets are the standard deviation

	Porosity (vol.%)	Total pore surface area (m^2/g)
CO*	23.34 (±0.34)	0.674 (±0.28)
IP	22.82 (±0.40)	1.955 (±0.41)

ET	21.85 (±0.51)	1.227 (±0.45)
W	19.36 (±0.38)	1.393 (±0.36)
WIP	17.87 (±0.71)	1.328 (±0.51)
WET	20.38 (±0.09)	1.29 (±0.21)

309

310

311 The MIP curves show that the porosity reduction in the samples treated with WIP and WET (Fig. 7d and 7e

312 respectively) can be attributed mainly to the reduction in the population of pores with larger diameter (17 to 100

313 µm). The reduction in larger pores in both samples is also accompanied by an increase of the intermediate pores

314 (diameters 1 to 10 µm). This effect is also observed for the sample treated with IP (Fig. 7a) although this sample

315 presents no visible reduction of the pores with larger diameter size (17 to 100 µm). In contrast, IP and W nanolimes

316 seem to be more effective in filling the pores with smaller size (0.05 to 0.7 µm), defining a new pores population of

317 diameter < 0.050 µm. These results suggest that nanolime in a water-alcohol solution tends to be more effective in

318 filling the larger pores than nanolime in alcohols only or in water only which, in contrast, favour an increase of the

319 surface area thanks to the presence of micropores, in accordance with previous results obtained from aqueous

320 nanolime suspension [33].

321

322
a) b)

323
c) d)

e)
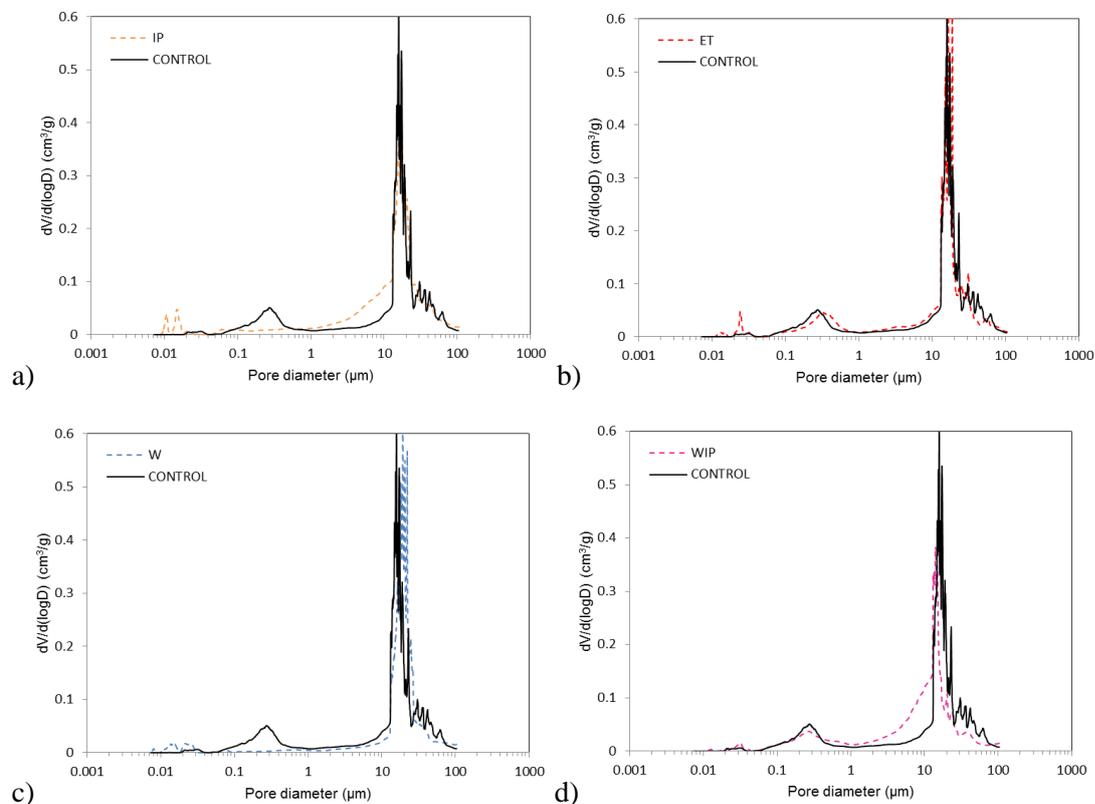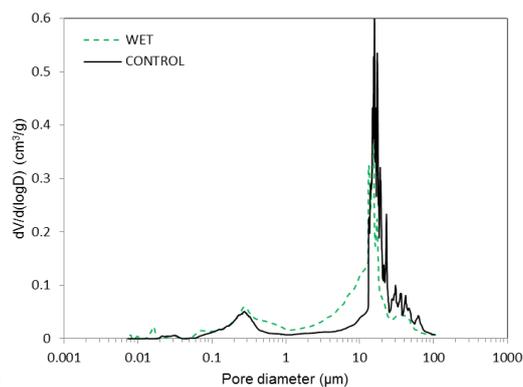
Figure 7. Pore size distribution of control and treated samples: a) IP; b) ET; c) W; d) WIP; and e) WET.

The water absorption and drying curves are reported in Fig. 8 and Fig. 9, and water absorption and drying characteristics are reported in Table 5. The denser pore structure at the surface slightly affected the water absorption and drying kinetics of the samples. Results show that all treatments slightly delayed the water absorption by capillary compared to control samples (Fig 8). WIP and W seem to present the higher reduction of the water absorption by capillary curves than the other treatments. All treated samples also presented a decrease of the water absorption coefficient (WAC), although the high standard deviation makes this decrease not statistically significant (Table 5). This decrease of the water absorption by capillary is due to a reduction of the porosity at the mortar's outer 1cm (MIP and DRMS analysis), which slows down the capillary rise [49]. WIP and W samples required more time (30 minutes more) to reach the asymptotic values than the other treatments (Fig. 8). All treated samples also presented a decrease of the water absorbed at asymptotic value (Table 5), although the standard deviation also indicates that the decrease is not statistically significant. These results could be in accordance to the MIP results reported above which suggest that WIP and W treatments yielded higher reduction on porosity.

Table 5. Apparent porosity by immersion, water absorption and drying characteristics

Parameter	CO	IP	ET	W	WIP	WET
Capillary absorption coefficient (10^{-3}g/cm^2 s$^{0.5}$)	17,1 (± 2.74)	15,8 (±2.46)	13,7 (±2.24)	13,2 (±3.18)	12,1 (±2.28)	15,2 (±2.22)
Water absorbed at asymptotic value (g)	11.05 (± 0.49)	10.9 (±0.25)	10.85 (± 0.10)	10.36 (±0.40)	10.56 (± 0.56)	10.55 (± 0.53)
Initial drying rate (10^{-3}g/ cm^3 h)	4,3 (±0.3)	3,6 (±0. 3)	3,5 (±0. 2)	3,2 (±0. 2)	2,7 (±0. 2)	2,6 (±0. 2)
Time for total drying (h)	± 60	± 70	± 78	± 78	± 78	± 78

342
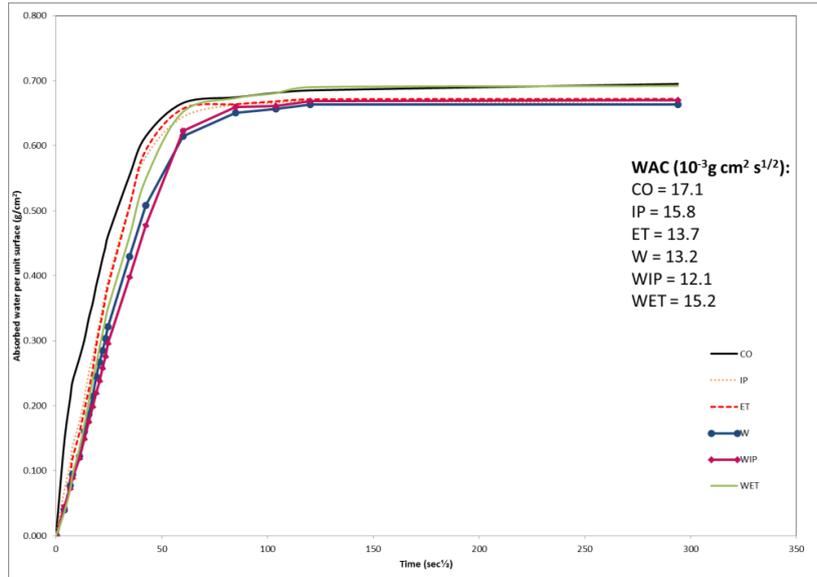
343

344   **Figure 8**. Capillary absorption curves of treated specimens (solvents).

345

346   The drying kinetics curves and the initial and final drying rates are shown in Fig. 9 and Table 5. Results showed

347   that all treatments slowed the initial drying rate of the specimens, which was also noticed in previous work [12, 27,

348   44]. This was attributed to the denser pore structure in the specimens' surface, which reduces the water transport

349   towards the surface slowing down the drying [12]. Control samples were completely dry after 60 hours. In contrast,

350   IP samples needed approximately 70 hours to dry while ET, W, WIP and WET samples needed more than 75 hours.

351
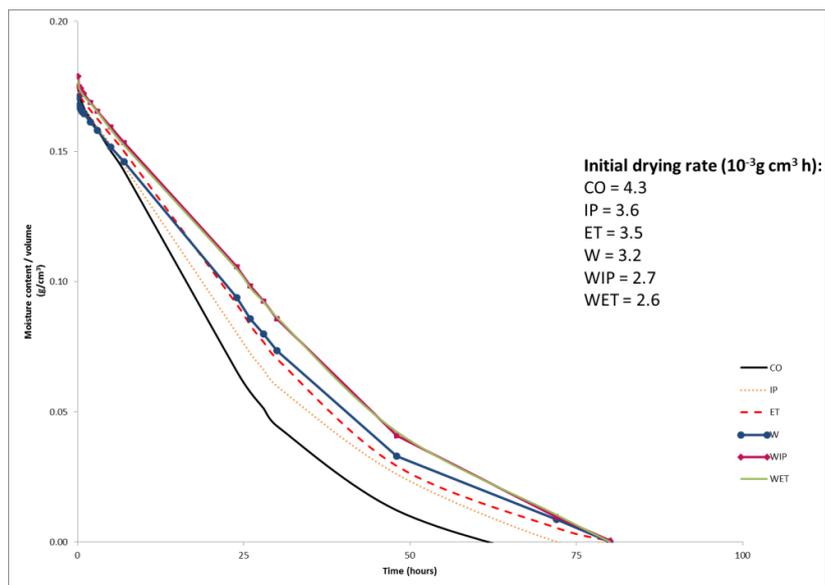
352

353   **Figure 9**. Drying curves of treated specimens (solvents).

354

The results of the Scotch Tape Test (STT) are shown in Table 6. All treatments resulted in a similar decrease of removed material ($\Delta W \approx 80\%$). These results confirm that the surfaces of all treated samples improved surface cohesion after nanolime treatments, regardless of the nanolime used.

Table 6. Scotch Tape Test (STT): experimental results

Code ID	Released material (mg/cm^2)	ΔW (%)	SD
CO	67.65	-	18.3
IP	9.42	86.1	3.6
ET	7.72	88.6	4.8
W	16.19	80.2	9.4
WIP	12.64	81.3	8.1
WET	15.8	80.9	6.2

Scotch area: 3 x 1.5 cm; SD (Standard Deviation) of released material

Drilling resistance results are shown in Figure 10. The control samples presented a constant drilling resistance (F ~ 0N (± 0.12)) throughout the drilling depth (20 mm). Results show that IP, ET, W and WET treatments clearly increase the drilling resistance of the mortar within about 2-3 mm from the surface more than an order of magnitude (up to a resistance of 1.5N). Additionally, a small consolidation effect (drilling resistance increased to F ~ 0.35N) is also noticeable up to a depth of 10 mm for these samples. The W sample yielded the highest increase in the drilling resistance in the outer 2-3 mm (>1.5 N). This is attributed to the high reactivity of the nanoparticles and the low kinetic stability of this suspension, which could facilitate the accumulation and carbonation of the nanoparticles on the surface. In contrast, the consolidation effect of WIP, which was found as the most stable nanolime suspension (Fig. 3), appears to be more homogeneous within a depth of 6-7 mm (Fig. 10d). This would be preferable as it does not result in the formation of a thin superficial layer which could increase the risk of spalling due to processes such as freeze-thaw or salt crystallization occurring beneath this layer. However, further research must be carried out to fully understand the penetration of these treatments.

Recent studies carried out by Borsoi et. al. [29, 30, 34] concluded that nanolime deposition in the pores can be influenced by the type of solvent. These researches concluded that nanoparticles tend to migrate back to the surface during the evaporation of the solvent, thus solvents with slower evaporation rate can enhance the deposition of

378　nanoparticles in the pores in highly porous substrates. In the present study, DRMS results show that there is not a

379　clear correlation between the evaporation rate of the solvent and the in-depth consolidation of nanolimes. The

380　addition of water to IP, which slows down the evaporation rate of the solvent, appears to have increased the

381　penetration and degree of consolidation. However, this effect was not seen for the samples treated with ET and

382　WET, where the addition of water to the ET solvent did not yield an increase in penetration and consolidation

383　degree. This could be attributed to the fact that the nanolime used by Borsoi et. al. was synthesised by solvothermal

384　reactions while the nanolime used in this work was prepared by an anion exchange process. Both types of

385　nanolimes present slightly different properties such as colloidal stability, reactivity and morphology [12, 21] which

386　could have affected their behaviour.

387

388　a) b)

389　c) d)

390
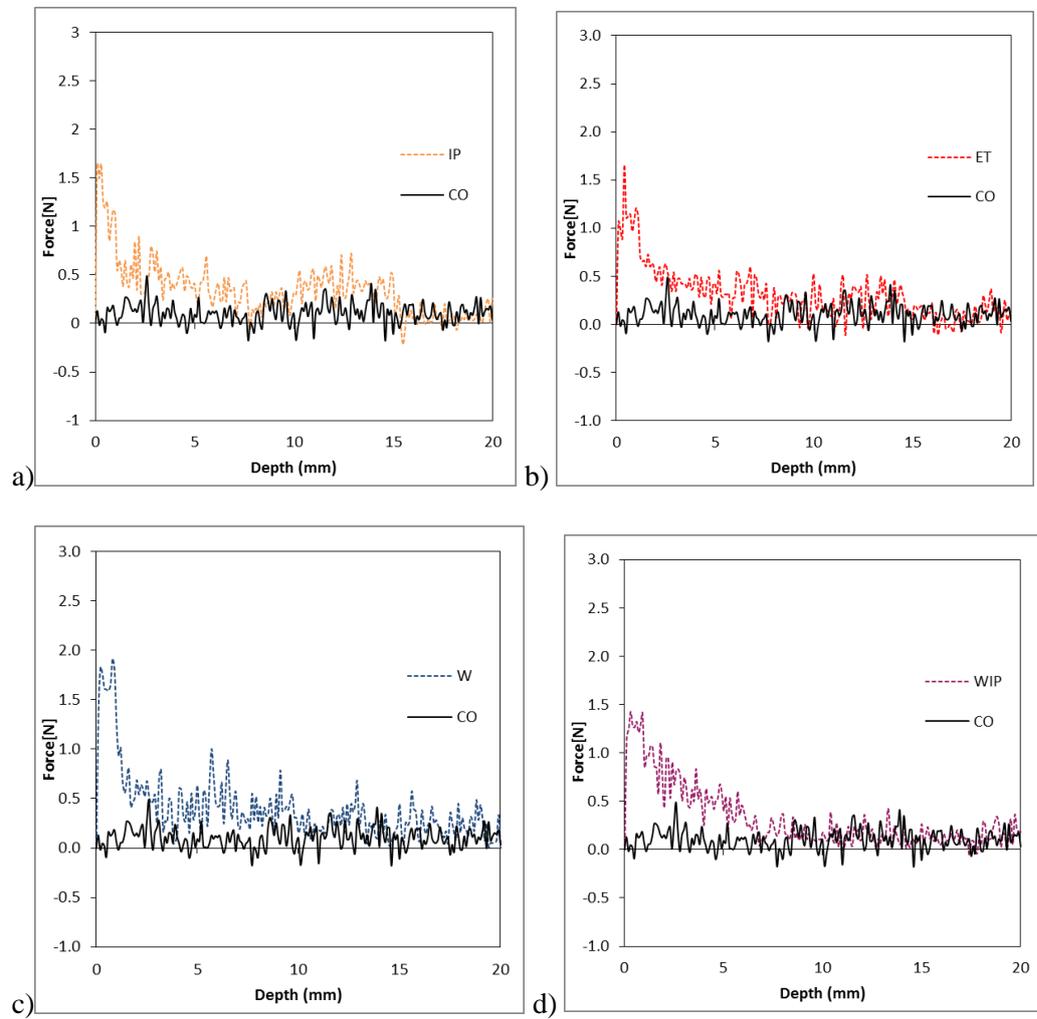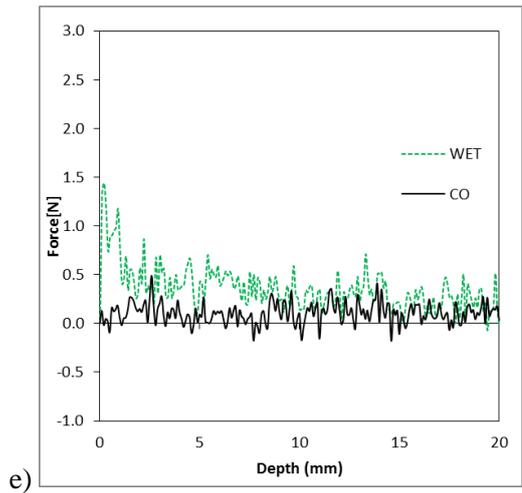
391   **Figure 10**. Drilling resistance profiles for control and treated samples: a) IP; b) ET; c) W; d) WIP; and e) WET.

392

393   Comparing the SEM images of control (Fig. 11a) and treated surface samples (Fig. 11b-f) show how the new

394   calcitic material fills the voids. These micrographs are in line with previous results of MIP and suggest a slight

395   reduction of the porosity of the mortar surface which is confirmed by STT showing that the surface is significantly

396   more compact after treatment as a result of the nanoline presence at the mortar's surface. The surface morphology

397   was significantly altered after the application of the nanolime treatments. Fig 11 shows how all nanolime

398   treatments covered the consolidated surface, which also modifies the aesthetic color of the substrates (see below

399   paragraph, colorimetric analysis).

400

401

402 c)

403 e)
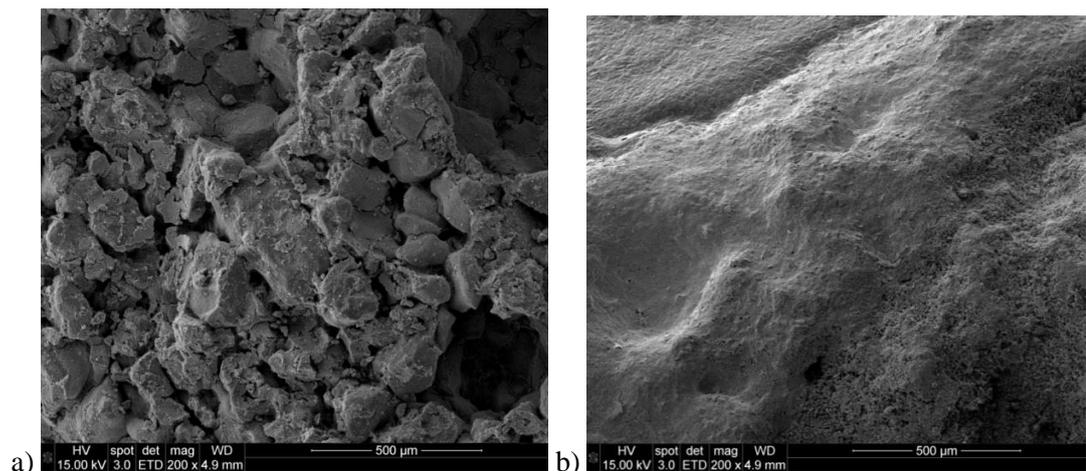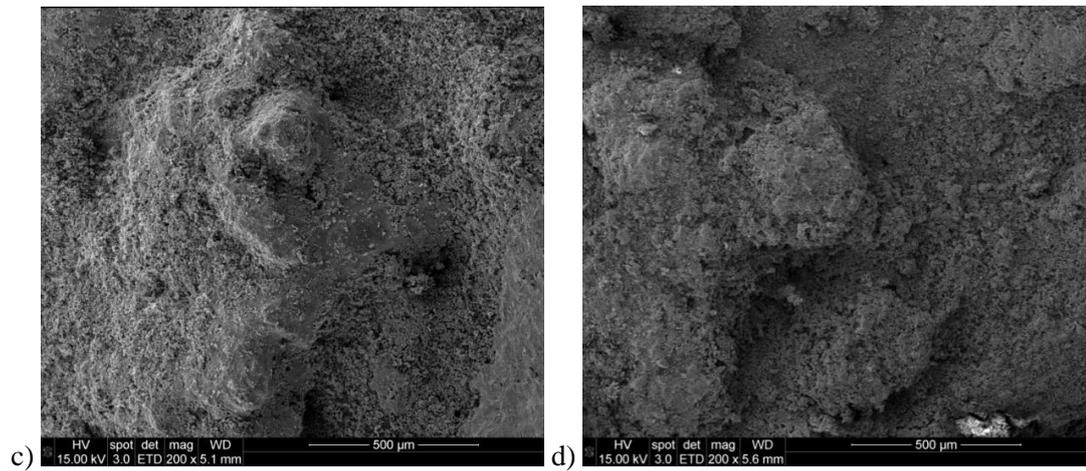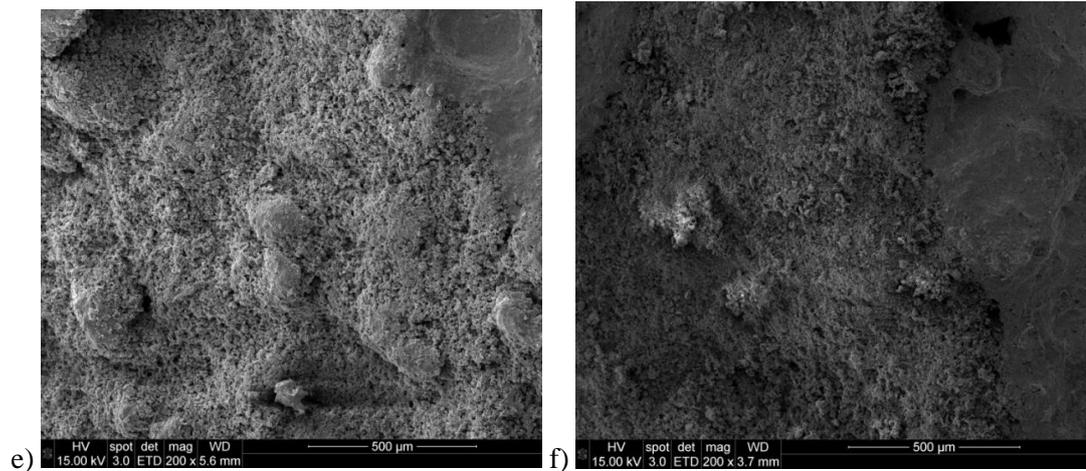
Figure 11. SEM micrographs of samples: a) control at 200x; b) IP sample at 200x; c) ET sample at 200x; d) W sample at 200x; e) WIP sample at 200x; f) WET sample at 200x.

A consolidation treatment should improve the physical-mechanical properties of a material a without changing its aesthetic appearance [43]. One of the most common nanolime side effects, which was already noticed in previous studies [12, 14; 32], is the whitening of the surface after treatment. Colorimetric results (Table 7) showed that all treatments, performed by brush, caused whitening of the specimens' surface above the $\Delta E=3$ threshold. WIP obtained the lowest whitening and chromatic variations ($\Delta L^* \sim 7$ and $\Delta E^* \sim 10$ values) compared to the other treatments. This could be attributed to the higher colloidal stability of this suspension which facilitates its penetration deeper into the pores thus reducing particle accumulation on the surface. However, previous research had confirmed that the aesthetic alteration decreases after several wet-dry cycles without affecting the mechanical properties [12].

Table 7. Chromatic alterations resulting from the applied treatments. Mean values determined from 30 measurements

	ΔL^*	Δa^*	Δb^*	ΔE^*

IP	13.72 (±0.89)	-1.78 (±0.13)	-7.96 (±0.43)	15.96
ET	11.97 (±1.97)	-1.64 (±0.28)	-7.69 (±1.22)	14.32
W	11.92 (±1.87)	-1.65 (±0.31)	-8.12 (±1.13)	14.52
WIP	7.81 (±1.78)	-0.18 (±3.92)	-6.79 (±1.12)	10.35
WET	11.02 (±2.25)	5.33 (±1.60)	-7.78 (±1.05)	14.50

417

418

4.2.4 Conclusions

420 The present study has shown that $Ca(OH)_2$ nanoparticles synthesised by anion exchange process and dispersed in

421 various types of solvents can be effective as a consolidation treatment for porous lime mortars or other calcareous

422 building materials when applied by brushing. It has been shown that all treatments reduced the porosity of the

423 external part of the mortar. WIP and W seem to yield a slightly higher reduction of porosity followed by WET. The

424 porosity reduction in samples treated with WIP and WET can be attributed mainly to the reduction in the

425 population of pores with larger diameter size (17 to 100 µm) while IP and W seem to be more effective in filling

426 the pores with smaller size (0.05 to 0.7 µm).

427 The denser pore structure at the surface slightly affected the water absorption of the treated samples showing that

428 they slightly delayed the water absorption by capillarity compared to control samples. WIP and W seems to present

429 higher reduction of the water absorption by capillarity than the other treatments. This result appears to be in

430 accordance with the MIP results reported above which suggest that WIP and W treatments yielded higher reduction

431 of the porosity.

432 All treated samples presented similar drying rates to each other and all needed more time to dry than the control

433 due to the denser pore network on the mortars' surface. This is not desirable as it could increase the risk of several

434 decay processes (e.g. spalling from freeze-thaw or biological growth).

435 All nanolime treatments increased the drilling resistance of the superficial mortar layer. DRMS results showed that

436 IP, ET, W and WET treatments clearly increased the drilling resistance of the mortar within about 2-3 mm from the

437 surface. Additionally, a light consolidation effect was also noticeable up to 10 mm for these samples. In contrast,

438 the consolidation effect of WIP appears to be more homogeneous within a depth of 6-7 mm which might be

439 attributed to the slightly slower evaporation rate of the azeotropic mixture. W sample presented the highest increase

440 in the drilling resistance in the outer 2-3 mm (>1.5 N), together with a slight increase up to about 20 mm. This can

441 be attributed to the high reactivity of the nanoparticles and the low kinetic stability of this suspension, which could

442 facilitate the carbonation of the nanoparticles on the surface. However, more research must be carried out to fully

understand the penetration and consolidation mechanism of the nanolime suspensions. Furthermore, research is needed to investigate the long-term performance of nanolime treatments focusing on possible weathering processes such as freeze-thaw or salt crystallization.

All treatments produced whitening of the substrate's surface after application by brush. WIP treatment yielded the lowest whitening and chromatic variations compared to the other treatments, which is slightly higher than the thresholds generally accepted ($\Delta E > 3$). The whitening effect associated with treatments decreased to values which are imperceptible to the naked eye after exposing the samples to the accelerating weathering test [12]. However, in order to fulfil the aesthetic compatibility requirements also in short times, a more in deep study of the application procedure should be performed.

According to the above results, in the conditions here described, the WIP treatment seems to present slightly better consolidating properties on the highly porous lime-mortars in terms of increased drilling resistance, higher reduction of porosity, higher delay of the water absorption by capillarity, and lower impact on aesthetic properties compared to the other suspensions. However, the data showed no drastic differences among the solvents, thus more research seems to be necessary to fully understand the influence of solvent on the consolidation effectiveness.

References

[1] Doehne E., Price C. A., (2010), "Stone Conservation: An Overview of Current Research", Research in conservation Series, Getty Conservation Institute, USA.

[2] ICOMOS, (1964), "The Venice Charter", International Charter for the Conservation and Restoration of Monuments and Sites.

[3] Wheeler G., (2005), "Alkoxysilanes and Consolidation of stone", Research in conservation Series, Getty Conservation Institute, USA

[4] Wheeler G., (2008), "Alkoxysilanes and the consolidation of stone: Where we are now. In Stone Consolidation in Cultural Heritage: Research and Practice", Proceedings of the International Symposium, Lisbon, 6-7 May 2008, ed. J. Delgado-Rodriguez and J. M. Mimoso, 41-52. Lisbon: LNEC (Laboratorio National de Engeneria Civil).

[5] Ferreira-Pinto, A. P. and Delgado-Rodrigues J., (2008), "Hydroxylating conversion treatment and alkoxysilane coupling agent as pre-treatment for the consolidation of limestones with ethyl silicate". In Stone Consolidation in Cultural Heritage: Research and Practice; Proceedings of the International Symposium, Lisbon, 6-7 May 2008, ed. J. Delgado-Rodriguez and J. M. Mimoso, 41-52. Lisbon: LNEC (Laboratorio National de Engenheria Civil).

[6] Pozo-Antonio, J.S., Otero.J, Alonso P., et al, (2019), Nanolime- and nanosilica-based consolidants applied on heated granite and limestone: Effectiveness and durability, Construction and Building Materials, 201, pp.852-870.

[7] Price, C., Ross, K., White, G., (1988), "A further appraisal of the 'Lime Technique' for limestone consolidation, using a radioactive tracer". IIC journal.Studies in Conservation, vol. 33 (4), pp.178–186.

[8] Clarke, B. L., and J. Ashurst, (1972), Stone Preservation Experiments. Watford: Building Research Establishment; London: Directorate of Ancient Monuments and Special Services.

[9] Sassoni, E., Naidu, S., Scherer, G.W., (2011), The use of hydroxyapatite as a new inorganic consolidant for damaged carbonate stones, Journal of Cultural Heritage, vol. 12, pp. 346–355.

[10] Natali, I., Tomasin, P., Becherini, F., Bernardi, A.,et al., (2015), Innovative consolidating products for stone materials: field exposure tests as a valid approach for assessing durability, vol. 3 (6), Heritage Science.

[11] Ambrosi, M., Dei L., Giorgi R., et al., (2001), "Colloidal particles of $Ca(OH)_2$: Properties and applications to restoration of frescoes", Langmuir, 17(14), pp.4251–4255.

[12] Otero J., Starinieri V., Charola A. E., (2018), "Nanolime for the consolidation of lime mortars: a comparison of three available products", Journal of Construction and Building Materials Vol. 181, pp.394-407.

[13] Rodriguez-Navarro C., Ruiz-Agudo E., (2017), "Nanolimes: from synthesis to application", Pure and Applied Chemistry, Volume 90, Issue 3, Pages 523–550, ISSN (Online) 1365-3075, ISSN (Print) 0033-4545, DOI: https://doi.org/10.1515/pac-2017-0506.

508

509 [14] Baglioni, P., Chelazzi D., Giorgi R., et al, (2014), "Commercial Ca(OH)$_2$ nanoparticles for the consolidation of

510 immovable works of art". Applied physics. A, Materials science & Processing, 114(3), pp.723–732

511

512 [15] Sequeira, S., Casanova C., Cabrita E. J., (2006), "Deacidification of paper using dispersions of Ca(OH)$_2$

513 nanoparticles in isopropanol", Journal Cultural Heritage, 7, pp.264–272.

514

515 [16] Giorgi R., Dei L., Ceccato M., et al, (2002), "Nanotechnologies for Conservation of Cultural Heritage: Paper

516 and Canvas Deacidification", Langmuir 18(21), pp.8198-8203. **DOI:** 10.1021/la025964d

517

518 [17] Natali I., Tempesti P., Carretti E., et al, (2014), "Aragonite Crystals Grown on Bones by Reaction of CO2 with

519 Nanostructured Ca(OH)$_2$ in the Presence of Collagen. Implications in Archaeology and Paleontology", Langmuir

520 30(2), 660-668.

521

522 [18] Poggi, G., Toccafondi N., Chelazzi D., et al, (2016), "Calcium hydroxide nanoparticles from solvothermal

523 reaction for the deacidification of degraded waterlogged wood". Journal of Colloid and Interface Science, 473,

524 pp.1–8.

525

526 [19] Borsoi G., Tavares M., Veiga R., et al, (2012), "Microstructural characterization of consolidant products for

527 historial renders: an innovative nanostructured lime dispersion and a more traditional ethyl silicate limewater

528 solution", Journal of microscopy Society of America, 18(5), pp. 1181-9.

529

530 [20] Costa D., Delgado-Rodrigues J., (2012), "Consolidation of a porous limestone with nano-lime", in: G. Wheeler

531 (Ed.), 12th International congress on the deterioration and conservation of stone, New York, pp. 10–19.

532

533 [21] Arizzi, A., Gomez-Villalba L. S., Lopez-Arce P., et al., (2015), "Lime mortar consolidation with

534 nanostructured calcium hydroxide dispersions: the efficacy of different consolidating products for heritage

535 conservation". European Journal of Mineralogy, 27(3), pp.311–323.

536

537 [22] Slizkova, Z., Dracky M., Viani A., (2015), "Consolidation of weak mortars by means of saturated solution of

538 calcium hydroxide or barium hydroxide", Journal of Cultural Heritage, vol. 16, No. 4, pp. 420-460.

539

540 [23] López-Arce, P., Gomez-Villalba L.S., Pinho L., et al., (2010), "Influence of porosity and relative humidity on

541 consolidation of dolostone with calcium hydroxide nanoparticles: Effectiveness assessment with non-destructive

542 techniques". Materials Characterization, 61(2), pp.168–184.

543

544 [24] Taglieri, G., Felice, B., Daniele, V., Volpe, R., Mondelli C., (2016), "Analysis of the carbonatation process of

545 nanosized Ca(OH)$_2$ particles synthesized by exchange ion process ". Proc Inst Mech Eng., 230, pp. 25-31.

546

547 [25] Dei, L., and Salvadori, B., (2006), "Nanotechnology in cultural heritage conservation: nanometric slaked lime

548 saves architectonic and artistic surfaces from decay". Journal of Cultural Heritage, 7(2), pp.110–115.

549

550 [26] Daniele, V., Taglieri, G., (2010), "Nanolime suspensions applied on natural lithotypes: The influence of

551 concentration and residual water content on carbonatation process and on treatment effectiveness". Journal of

552 Cultural Heritage, 11(1), pp.102–106.

553

554 [27] Otero J., Starinieri V., Charola A. E., (2019), "Influence of substrate pore structure and nanolime particle size

555 on the effectiveness of nanolime treatments", Journal of Construction and Building Materials 209, pp.701-708.

556

557 [28] Rodriguez-Navarro, C., Bettori I., Ruiz-Agudo E., (2016), "Kinetics and mechanism of calcium hydroxide

558 conversion into calcium alkoxides: Implications in heritage conservation using nanolimes", Langmuir, 32(20), pp.

559 5183-5194.

560

561 [29] Borsoi, G., Lubelli B., Van Hees R. et al., (2016a), "Effect of solvent on nanolime transport within limestone:

562 How to improve in-depth deposition". Colloids and Surfaces A: Physicochemical and Engineering Aspects, 497,

563 pp.171–181.

564

565 [30] Borsoi, G., Lubelli, B., van Hees, R. et al. (2016b), "Optimization of nanolime solvent for the consolidation of

566 coarse porous limestone", Appl. Phys. A (2016) 122: 846. https://doi.org/10.1007/s00339-016-0382-3

567

568 [31] Taglieri G, Daniele V., Macera L., Mondelli C., (2017), "Nano $Ca(OH)_2$ synthesis using a cost-effective and

569 innovative method: Reactivity study", J Am Ceram Soc. 2017;100:5766–5778

570
571 [32] Taglieri G., Otero J., Daniele V., et. al., (2017), "The biocalcarenite stone of Agrigento (Italy): Preliminary

572 investigations of compatible nanolime treatments", Journal of Cultural Heritage

573

574 [33] Daniele V., Taglieri G., Macera L., et al (2018), Green approach for an eco-compatible consolidation of the

575 Agrigento biocalcarenites surface, Construction and Building Materials vol. 186, pp.1188-1199

576

577 [34] Borsoi G., Lubelli B., Van Hees R.P.J., et al, (2015), "Understanding the transport of nanolime consolidants

578 within Maastricht limestone", Journal of Cultural Heritage, pp. 1296-2074. DOI: 10.1016/j.culher.2015.07.014

579

580 [35] EN 1015-3:1999, The European Standard, (1999), Methods of test for mortar for masonry. Determination of

581 consistence of fresh mortar (by flow table).

582

583 [36] EN 1015-2:1998, The European Standard, (1998), Methods of test for mortar for masonry. Bulk sampling of

mortars and preparation of test mortars.

[37] Rietveld H.M., (1969), "A profile refinement method for nuclear and magnetic structures", Journal Applied Crystallography, 10, 65.

[38] Bish D. L. and Post J. E., (1989), Modern powder diffraction. Mineralogical Society of America, Crystal Reasearch & Technology, Washington. ISBN 0‑939950‑24‑3.

[39] Volpe R., Taglieri G., Daniele V., et. al., (2016), "A process for the synthesis of $Ca(OH)_2$ nanoparticles by means of ionic exchange resin", European patent EP2880101.

[40] Taglieri, G., Daniele V., Del Re G., Volpe, R., (2015), "A new and original method to produce $Ca(OH)_2$ nanoparticles by using an anion exchange resin". Advances in Nanoparticles, 4, pp.17–24.

[41] Taglieri, G., Daniele, V., Macera, L., (2019), Synthesizing alkaline earth metal hydroxides nanoparticles through an innovative single-step and eco-friendly method, Solid State Phenom., vol. 286, pp. 3–14.

[42] Otero J., Charola A. E., Grissom C. A., Starinieri V., (2017), "An overview of nanolime as a consolidation method for calcareous substrates", GE-Conservacion, 1 (11), 71-78pp.71-78

[43] Rodriguez-Navarro C., Suzuki A., Ruiz-Agudo E., (2013), "Alcohol dispersions of calcium hydroxide nanoparticles for stone conservation", Langmuir vol. 29, pp. 11457−11470.

[44] Otero J., Charola A. E., Starinieri V., (2019), Sticky rice–nanolime as a consolidation treatment for lime mortars, Journal of Material Science, Vol. 54, Issue 14, pp. 10217-10234.

[45] EN 16322. (2013), The European Standard CEN - Conservation of Cultural Heritage - Test methods - determination of drying properties.

[46] EN 13755, (2008), The English Standard for Natural stone test methods. Determination of water absorption at atmospheric pressure.

[47] ASTM C 67-00: Standard Test Methods for Measuring Apparent Porosity at atmospheric pressure, (2000), ASTM

[48] ASTM D3359-02: Standard Test Methods for Measuring Adhesion by Tape Test, (2002), ASTM International, 10 August.

622   [49] Charola A. E. and Wendler E., (2015), "An overview of the water-Porous building materials interactions",

623   Restoration of Building and Monuments Journal, vol. 21(2-3), pp. 55-63.

624

625

626

627

628

629

630

631

632

633

634

635

636

637

638